FASH and MASH: *F*emale and *M*ale *A*dult human phantoms based on polygon me*SH* surfaces
Part I: Development of the anatomy

V F Cassola[1], V J de Melo Lima[2], R Kramer[1] and H J Khoury[1]

[1] Department of Nuclear Energy, Federal University of Pernambuco, Avenida Prof. Luiz Freire, 1000, CEP 50740-540, Recife, Brazil
[2] Department of Anatomy, Federal University of Pernambuco, Avenida Prof. Moraes Rego, 1235, CEP 50670-901, Recife, Brazil

Statement of provenance:
'This is an author-created, un-copyedited version of an article accepted for publication in Physics in Medicine and Biology. IOP Publishing Ltd is not responsible for any errors or omissions in this version of the manuscript or any version derived from it. The definitive publisher authenticated version is available at: doi:10.1088/0031-9155/55/1/009. '

Abstract

Among computational models, voxel phantoms based on computer tomographic (CT), nuclear magnetic resonance (NMR) or colour photographic images of patients, volunteers or cadavers became popular in recent years. Although being true to nature representations of scanned individuals, voxel phantoms have limitations, especially when walled organs have to be segmented or when volumes of organs or body tissues, like adipose, have to be changed. Additionally, the scanning of patients or volunteers is usually made in supine position, which causes a shift of internal organs toward the ribcage, a compression of the lungs and a reduction of the sagittal diameter especially in the abdominal region compared to the regular anatomy of a person in upright position, which in turn can influence organ and tissue absorbed or equivalent dose estimates. This study applies tools developed recently in the areas of computer graphics and animated films to the creation and modelling of 3D human organs, tissues, skeletons and bodies based on polygon mesh surfaces. Female and male adult human phantoms, called FASH (*F*emale *A*dult me*SH*) and MASH (*M*ale *A*dult me*SH*), have been designed using software, like MakeHuman, Blender, Binvox and ImageJ based on anatomical atlases, observing at the same time organ masses recommended by the International Commission on Radiological Protection for the male and female reference adult in report No. 89. 113 organs, bones and tissues have been modelled in the FASH and the MASH phantoms representing locations for adults in standing posture. Most organ and tissue masses of the voxelized versions agree with corresponding data from ICRP89 within a margin of 2.6%. Comparison with the mesh-based male RPI_AM and female RPI_AF phantoms shows differences with respect to the material used, to the software and concepts applied and to the anatomies created.

1. Introduction

After having been exposed to low levels of ionizing radiation, a chest radiograph for example, human tissue located beneath the surface cannot express itself in terms of absorbed or equivalent dose visible to

the human eye or to a detector positioned at the surface. This fact creates a fundamental problem for dosimetry applied to radiation protection and has consequently led to the development of human phantoms, i.e. physical or computational representations of the human body to be used for the determination of absorbed or equivalent dose to radiosensitive organs and tissues. This development started almost 60 years ago with a simple homogeneous water phantom and has now arrived at anthropomorphic representations of the human body exhibiting unprecedented anatomical sophistication.

1.1 Computational phantoms

Progressive improvement of modelling the human anatomy has had a formative influence on the development of computational phantoms. Early radiation transport studies were using semi-infinite homogeneous 30 cm slab phantoms (Snyder 1950, Alsmiller and Moran 1968, Alsmiller et al 1970, Beck 1970, Irving et al 1967), then homogeneous elliptical cylinders (Auxier et al 1969, Sidewell et al 1969, Snyder 1971), also with embedded inhomogeneous parts to simulate the lungs (Sidewell and Burlin 1973), later a homogeneous (Snyder 1965) and finally a heterogeneous human phantom, which became known as the MIRD5 phantom (Snyder et al 1968, 1978). Body and organs of this stylized human phantom and of its derivations (Cristy 1980, Kramer et al 1982, Stabin et al 1995) were based on mathematical equations of geometrical bodies, like ellipsoids, truncated cones, tori, planes and intersections between them. Obviously, the geometrical representation of organs was quite simple and complicated anatomical structures, like the G.I. tract, could not be modelled with these geometrical surfaces, but on the other hand body dimensions and organ volumes could easily be changed if necessary. Although being anatomically not very accurate, stylized phantoms provided nevertheless reasonable absorbed or equivalent dose estimates for external and internal exposure. Stylized MIRD5-type phantoms have widely been used and some reports of the International Commission on Radiological Protection (ICRP) contain data, which have been calculated based on stylized phantoms, for example, conversion coefficients for external exposure released in Publication 74 (ICRP 1996).

Driven by the idea to design a model that looks like a real human, researchers took advantage of progress made in computer development and image processing to steadily improve the anatomy of the human phantoms. Voxel phantoms based on computer tomographic (CT), nuclear magnetic resonance (NMR) or colour photographic images of humans represent an important step towards the realization of that idea. Compared to the stylized MIRD5-type phantoms, voxel phantoms are basically true to nature representations of the individuals, which are represented in the images. Developed first independently by Gibbs et al (1984) and Williams et al (1986), many voxel phantoms have been created since then for male and female adults as well as for children based on organ and tissue segmentation in digital images of patients, volunteers or cadavers: The paediatric BABY and CHILD phantoms, as well as the adult DONNA, FRANK, HELGA, IRENE, GOLEM and LAURA phantoms (Zankl et al 1988, 2002, Petoussi-Henss et al 2002, Fill et al 2004, Petoussi-Henss and Zankl 1998, Zankl and Wittmann 2001), the paediatric UF newborn, 2 and 9 month, 4, 8, 11 and 14 year phantoms (Nipper et al 2002, Lee et al 2005), the Yale adult phantoms (Zubal et al 1994, Dawson et al 1997, Sjogreen et al 2001), the VIP-Man phantom (Xu et al 2000), the adult NORMAN and NAOMI phantoms (Dimbylow 1997, 2005, Jones 1997), the adult NORMAN-05 phantom (Ferrari and Gualdrini 2005), the adult MAX, FAX, MAX06 and FAX06 phantoms (Kramer et al 2003, 2004, 2006a), the ADELAIDE torso phantom (Caon et al 1999), the Japanese adult Nagaoka Man, Nagaoka Woman, Otoko, Onago, JM, and JF phantoms (Nagaoka et al 2004, Saito et al 2001, Sato et al 2007 a,b), the Korean KORMAN phantoms (Lee and Lee 2004) and the Chinese adult voxel phantom (Zhang et al 2007), to mention the most important ones. Recently, an excellent review paper on computational phantoms has been published by Zaidi and Xu (2007) and comprehensive information on this subject is given in the Handbook of Anatomical Models for Radiation Dosimetry (Xu and Eckerman 2009). Two specific adult voxel phantoms, REX and

REGINA, which are based on the GOLEM and the LAURA phantoms, will be published by the ICRP to be used by the scientific community as reference computational phantoms (ICRP 2009) for internal and external exposure.

Although providing anatomically improved representations of the human body, voxel phantoms still have their limitations. For example, depending on the voxel resolution, it is sometimes difficult or even impossible to correctly segment certain tissues, like the walls of the colon or the small intestine and/or their twists and turns. Also, image contrast of the CT images is often not sufficient for clearly segmenting boundaries between organs and tissues. Changing volumes of organs is possible but becomes a laborious process of voxel exchange with neighbouring tissues in 2D images, which can easily cause distortions in the 3D representation.

In 2001, Segars introduced a Cardiac-Torso phantom based on CT images from the Visible Human Project (available from http://www.nlm.nih.gov/research/visible) using non-uniform rational B-spline (NURBS) surfaces, a mathematical modelling tool frequently used in computer graphics and animated films, thereby showing a method how to overcome the above mentioned limitations of voxel phantoms. Using NURBS surfaces, 'hybrid' computational whole body phantoms for the newborn based on digital images were presented by Lee et al (2007a), which "preserve both the anatomical realism of voxel phantoms and the flexibility of stylized phantoms". Using the NURBS technique, organ volumes and /or body stature can easily be adjusted and at the same time a significantly higher degree of anatomical realism can be achieved (Lee et al 2007b, 2008, Johnson 2009). In order to correct the back and buttock region of a Korean adult male voxel phantom, Jeong et al (2008) used polygon mesh and NURBS surfaces, while Santos and Frère (2007a, b) constructed an adult male phantom using box modelling of primitives with Blender (2009) based on photographic images of a skeleton and on anatomical atlases.

Important contributions to human phantom design using software developed in computer graphics and animated films came from the research group of G. Xu at the Rensselaer Polytechnic Institute (RPI) in Troy, USA. First, a mesh-based method, called boundary representation, was used by Xu et al (2007) to design pregnant female phantoms in different gestational stages based on CT images of a pregnant woman, on cross-sectional images of the VIP-Man model (Xu et al 2000) and on polygon mesh models of organs downloaded from the internet. Then, the mesh-based concept for human phantom design was further developed by the RPI research group (Xu et al 2008, Zhang et al 2008a, b, Na et al 2008), which led to the publication of the adult male and female mesh-based phantoms, called RPI_AM and RPI_AF (Zhang et al 2009), which are based on surface mesh models for organs downloaded from the internet and adjusted to match organ mass specifications given by ICRP89 (ICRP 2002). Organ and tissue positions in the RPI_AM and RPI_AF phantoms correspond to humans in standing posture.

1.2 The purpose of this study

CALDose_X is a software tool made recently available to the public (www.grupodoin.com), which calculates organ and tissue absorbed doses, as well as radiation risks for patients being submitted to examinations in X-ray diagnosis based on Monte Carlo calculations using the MAX06 and the FAX06 phantoms (Kramer et al 2006a, 2008). The two phantoms have body heights, body weights, as well as organ and tissue masses in agreement with data recommended by the ICRP for the Caucasian male and female reference adults, which are considered to be 35 years old (ICRP 2002). However, real patients are often slimmer or fatter, smaller or taller or younger or older than a person simulated by the MAX06 or the FAX06 phantom. For given exposure conditions, organ and tissue absorbed doses, and consequently

radiation risks are influenced primarily by weight (fat distribution), followed by variations of the body height and finally by effects due to the adult aging process.

In order to make CALDose_X more patient-specific, a phantom development project based on the MAX06 and the FAX06 phantoms was initiated at the Department of Nuclear Energy at the Federal University of Pernambuco in Recife/Brazil, whose objective is to provide a series of 32 human adult phantoms, 16 for each sex, as a function of 4 different body weights and 4 different body heights, thereby focusing on the two most important anatomical parameters influencing organ and tissue absorbed doses and omitting the adult aging-related effects for the time being. Consequently, the objective is to change especially the fat distribution and the body height of the MAX06 and the FAX06 phantoms, a task one would preferably tackle with one of the above mentioned methods developed in the area of computer graphics.

Taking advantage of this situation, the MAX06 and the FAX06 phantoms were critically reviewed to find out if any organs or tissues require anatomical revision. It was found that due to the supine position of the individual during scanning first, the locations of the following organs were too elevated for an upright standing person: Lungs, liver, stomach, small intestine (SI), colon, uterus, ovaries, urinary bladder and prostate and second, by gravitation a part of the abdominal subcutaneous adipose was shifted sideward, thereby reducing the sagittal diameter especially in the abdominal region. Also, the SI was segmented in the abdomen with wall and contents voxels randomly distributed throughout the SI volume, because at the time it was not possible to segment the twists and turns of this walled organ. The tube of the colon showed discontinuities. The connection between stomach and SI was not defined. In the skeletons, some cervical vertebrae were too thick; the pelvises were too small, especially for the female phantom and parts of the lower ribs were not clearly defined. Also, the number of bone sites was considered to be too small. Finally, the body shapes of the MAX06 and the FAX06 phantoms were plump and parts of their faces, like ears, eyes, noses and lips were not visible.

In view of the number of organs to be moved and/or to be corrected, but especially because of the revision of the skeletons, of the phantoms' fat and muscle distributions and of the make-up of the surfaces, it was decided not to update the MAX06 and the FAX06 phantoms, but to design completely new phantoms. Freely available software tools using polygon mesh surfaces, like MakeHuman (2009) and Blender (2009) were employed to design two adult phantoms with organs and tissues based on anatomical atlases or on freely available 3D surfaces, while observing organ and tissue masses recommended by ICRP89 (2002). The new phantoms are called FASH (*F*emale *A*dult me*SH*) and MASH (*M*ale *A*dult me*SH*). They not only replace the FAX06 and the MAX06 phantoms, but they also become the starting points for the development of a series of phantoms with variable weight and height in the future.

2. Materials and methods

2.1 Materials

Normally, the raw material for the development of voxel phantoms consists of CT, NMR or photographic images of patients, volunteers or cadavers. Organs, tissues, skeleton and skin are segmented in these images and a continuous sequence of such segmented images represents a voxel phantom. However, in recent years, numerous websites for all kinds of 3D object have appeared on the internet, some of which offer 3D models of human anatomy. This study gives up on the use of CT or NMR images from humans as raw material for phantom construction, except for representing the trabecular bone structure. The two phantoms presented here are based on 3D anatomical models downloaded freely from the internet or on

organs and tissues modelled from scratch with appropriate open source software using polygon mesh surfaces. “A polygon mesh or unstructured grid is a collection of vertices, edges and faces that defines the shape of a polyhedral object in 3D computer graphics and solid modelling” (Wikipedia 2009). In both cases, atlases of anatomy provided the information necessary for the design of organs and tissues as well as for assembling them anatomically in a correct manner (Sobotta 2006, Wolf-Heidegger 2006).

Table 1. Organs and tissues modelled in the FASH and the MASH phantoms.

Organs downloaded from the internet	Organs and tissues	developed with	3D modelling
Stomach wall	Thymus	Eyes	Skin
Brain	Spleen	Small intestine wall	Adipose
Skeleton	Tongue	Colon wall	Muscle
Uterus	Nasal passage	Prostate	Spinal chord
Ovaries	Mouth cavity	Testes	Soft tissue*
Heart wall	Pharynx	Penis	Trachea
Liver	Larynx	Breasts	Thyroid
Teeth	Salivary glands	Adrenals	Urinary bladder wall
Kidneys	Esophagus	Lymphatic nodes	Gallbladder wall
	Lungs	Pancreas	

* Soft tissue: blood, blood vessels, connective tissue, muscular fascia, tendons, etc.

The FASH and the MASH phantoms consist of the organs and the tissues mentioned in table 1, most of which are relevant for the calculation of the effective dose (ICRP 2007). Brain (Artist-3D 2009), heart wall (Heart 3dxtras 2009), liver (Inria_Y5820 2009), kidneys (Inria_Y5733 2009), stomach wall (Inria_stomach 2009), uterus + ovaries (Inria_Y6003 2009), teeth (Teeth 3dxtras 2009) and the skeleton (Free 3D Models 2009) have been designed based on the 3D anatomical models downloaded from the internet and are shown in figure 1. All other organs and tissues were created based on 3D primitives and Bezier curves using 3D modelling. The surfaces of the phantoms were based on a 3D human model (MakeHuman 2009) presented in figure 2.

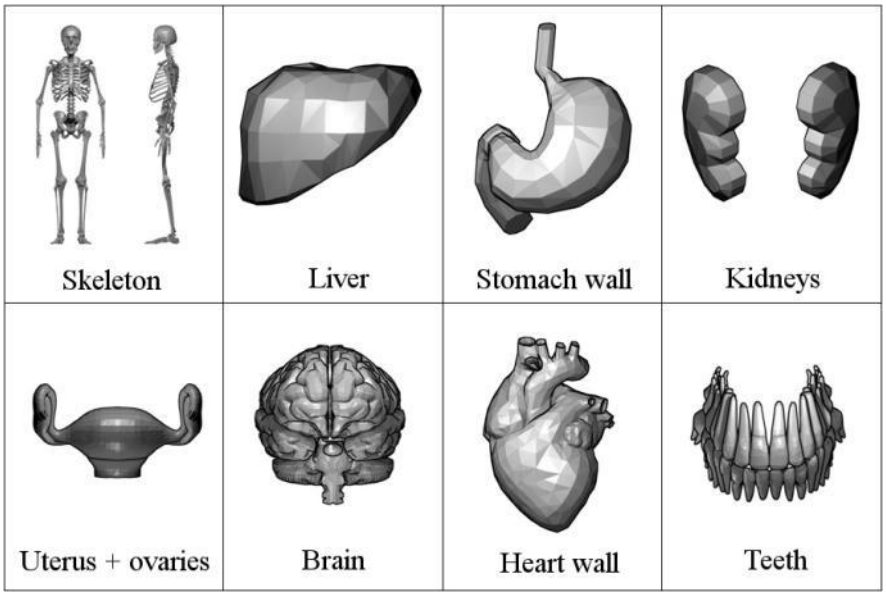

Figure 1. 3D anatomical models of eight organs and the skeleton downloaded from the internet

Figure 2. Basic humanoid 3D surface model of the MakeHuman software tool (MakeHuman 2009)

2.2 3D modelling tools

The methods used to construct the FASH and the MASH phantoms were the design and the editing of 3D surfaces and objects using the following free, open source software tools:

a) MakeHuman 0.9.1 RC1. For modelling of 3D humanoid characters based on a single and highly optimized mesh. The modelling is performed by deforming the mesh using an intuitive interface with the controls: age/sex, body mass, breast and body shape (MakeHuman 2009)

b) Blender, version 2.48. For modelling, animating and other applications, like the support for a variety of geometric primitives, including poly meshes, Bezier curves, NURBS surfaces and digital sculpting (Blender 2009).

c) Binvox. Software for reading a 3D model file and writing the information into a voxel file (Min 2009, Nooruddin and Turk 2003)

d) ImageJ. Java-based image processing program for 3D voxel volume adjustment developed by the National Institute of Health (ImageJ 2009). Customized analysis and processing can be made by addition of Java-based plugins and/or macro language.

2.3 Step by step construction of the phantoms

2.3.1 The surface

Using the MakeHuman software, the design of the 3D phantom surface starts with the basic humanoid model included in MakeHuman and shown in figure 2. Using the different control elements age/sex, body mass, breast and body shape shown on the left of the interface, preliminary body surfaces for FASH and MASH have been created using the body dimensions of the FAX06 and the MAX06 phantoms as guidance. Figures 3a and 3b show the early versions of the phantoms.

Figure 3a. MakeHuman version of the FASH surface

Figure 3b. MakeHuman version of the MASH surface

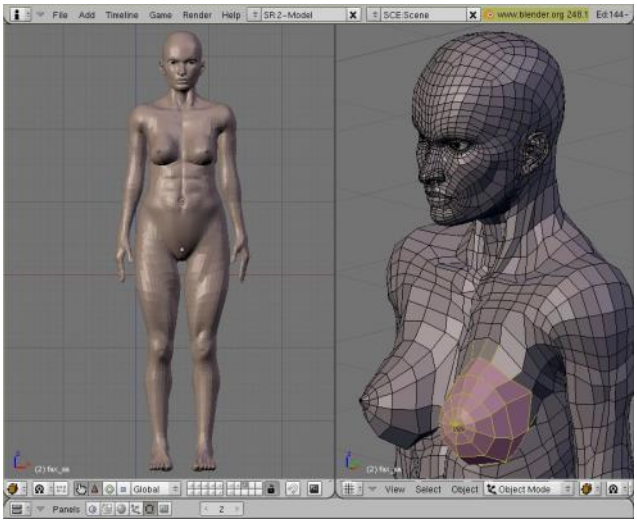

Figure 4. FASH surface imported into the Blender software showing the polygon mesh wireframe.

Next, the arms were straightened along the sides of the body and both surfaces were then exported as WaveFront file to the Blender software for further editing based on polygon mesh surfaces shown for the FASH phantom in figure 4. Changes of the body surface can now easily be done in any desired region of the body by moving the control points of polygon mesh wireframes. The process of surface modelling with MakeHuman and Blender can be seen in a 2.5 minute video attached to this paper.

2.3.2 The skeleton

The skeleton was modelled and introduced into the 3D phantom surface. The downloaded skeleton received an anatomically improved version of the spine and the sacrum (Inria_Y6396 2009), paranasal sinuses were added to the skull and different pelvises were designed for the male and the female phantoms. Position and shape of all bones were anatomically reviewed.

2.3.3 Organs

For the design of the internal soft tissue organs, the body was divided into four regions: head, thorax, upper abdomen and lower abdomen. All organs within a region were modelled simultaneously in order to ensure their correct anatomical positions relative to each other. The organs were designed based on the models shown in figure 1 or with design tools of the Blender software.

2.3.3.1 Head

First, the brain from figure 1 was adjusted to fit into the cavity of the skull. Then other organs, like salivary glands, eyes, tongue, nasal passage, larynx and pharynx were added using the digital sculpturing option of the Blender software. Figure 5 shows some organs of the head, both for males and females.

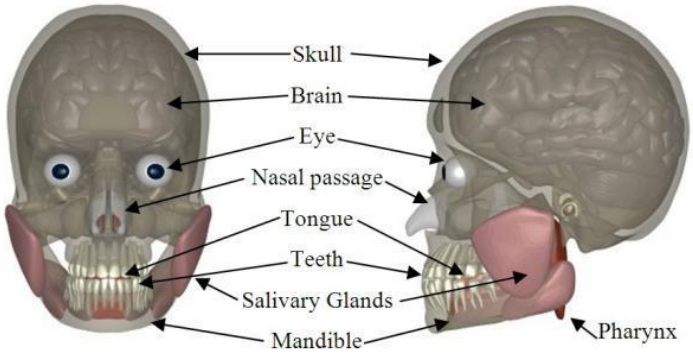

Figure 5. Head

2.3.3.2 Thorax region

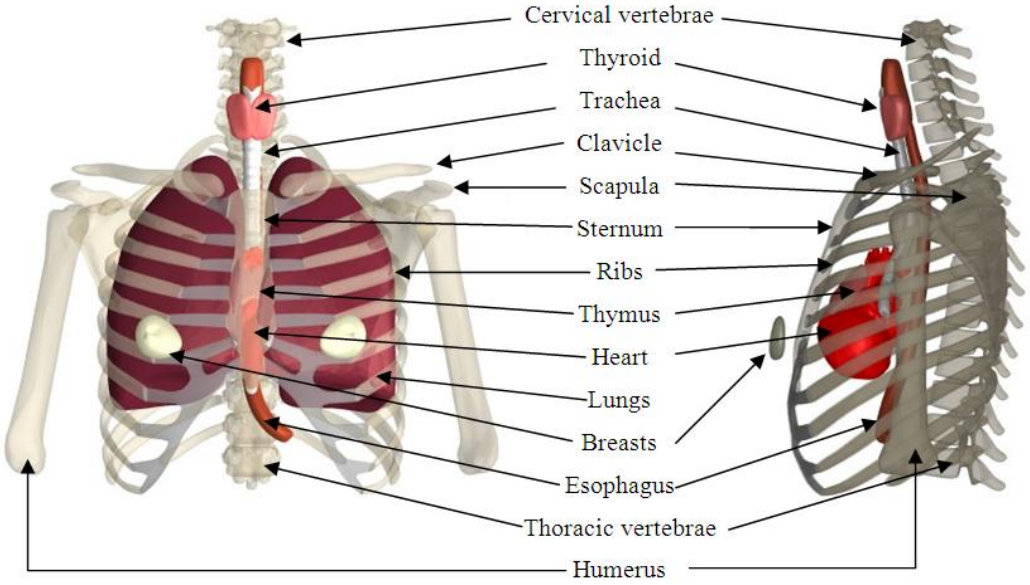

Figure 6. Male thorax region

The heart wall was based on the model shown in figure 1, while auricles and ventricles were designed based on a study developed at the Institute for Computational Engineering and Sciences and the Department of Computer Sciences at the University of Texas at Austin (Heart model 2009). Trachea and oesophagus were designed using Bezier curves and 3D modelling. The volume of the lungs was adjusted to fit into the ribcage. Figure 6 presents the male thorax region with its soft tissue organs. Females have the same organs, except for the size.

2.3.3.3 Upper abdominal region

From the organs of the upper abdominal region, liver, stomach and kidneys were based on the downloaded models shown in figure 1. The other organs were created using geometrical primitives, subdivision and finally digital sculpturing of the Blender software. Males and females have the same organs, except for the size, and are shown in figure 7.

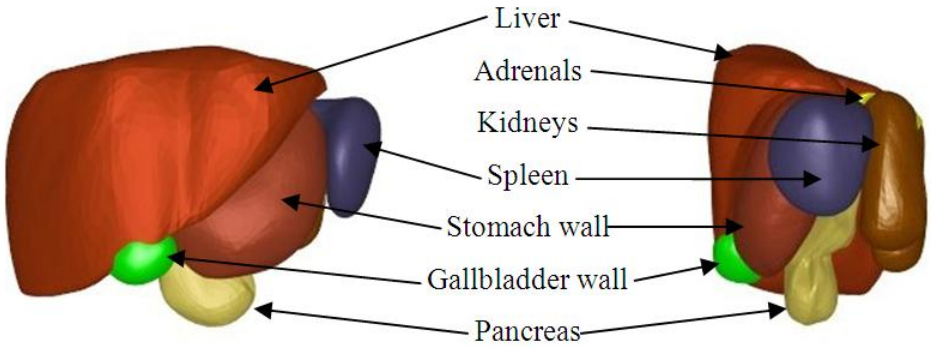

Figure 7. Upper abdominal organs

2.3.3.4 Lower abdominal region

In this region, females and males have partly different organs. Figure 8 shows the organs located in the lower female abdomen with ovaries, uterus and a larger pelvis. For the uterus and ovaries the model from figure 1 was used. Figure 9 presents the male version of the lower abdomen with prostate, testes and penis. The colon and the small intestine were designed with Bezier curves and the technique of extrusion, while the other organs were modelled based on geometrical primitives, extrusion and subdivision.

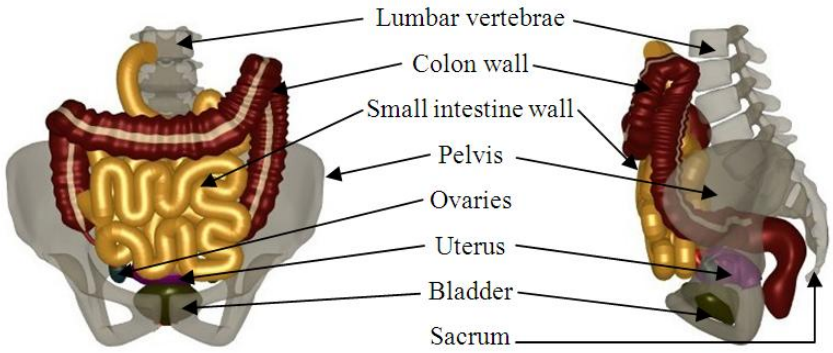

Figure 8. Female lower abdominal organs

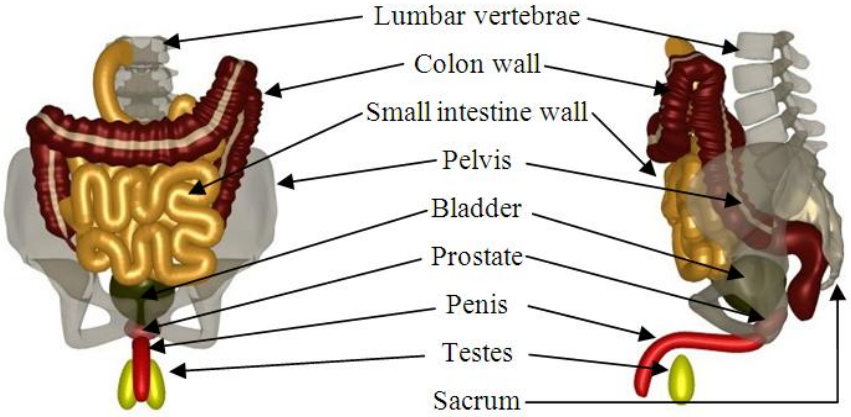

Figure 9. Male lower abdominal organs

2.3.4 Soft tissues

2.3.4.1 Lymphatic nodes

The lymphatic nodes were designed using the DupliVert tool of the Blender software. DupliVert comes from *Dupli*cation at *Vert*ices and represents a method which duplicates all vertices of the polygon mesh of a 3D object. Used together with the subdivision tool of Blender, DupliVert facilitates the positioning of the lymphatic nodes and guarantees that all nodes have the same size. Figure 10 shows the lymphatic nodes for the MASH phantom.

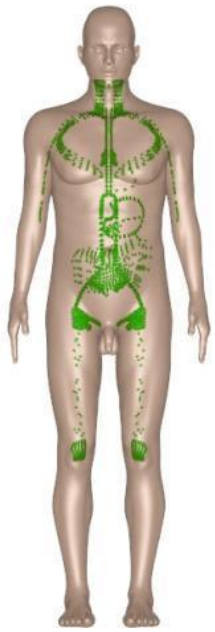

Figure 10. Lymphatic nodes in the MASH phantom

2.3.4.2 Muscle tissues

Figure 11. Muscle tissue in the FASH phantom

Using geometrical primitives, poly modelling, subdivision and digital sculpturing of the Blender software, the muscle tissue was modelled close to the skeleton, shown in figure 11 for the FASH phantom. During mesh volume adjustment, inevitable overlaps between neighbouring organs and tissues occur. These cases were identified and corrected with the Boolean operator of the Blender software.

2.3.5 Voxelization and volume adjustment

The dosimetric calculations presented in part II of this study were made using the EGSnrc Monte Carlo (MC) code (Kawrakow and Rogers 2003) applied to voxelized phantom geometry (Kramer et al 2006b, 2007, 2009b). Unlike the MC codes GEANT4 (available from: geant4.slac.stanford.edu/SLACTutorial07/Geometry1.ppt) or PENELOPE (Badal et al 2008), the EGSnrc code cannot be directly connected to 3D objects based on NURBS or polygon mesh surfaces. But even if this were possible, here it would not be helpful, because the skeletal dosimetry method used for the FASH and the MASH phantoms is based on digital μCT images of trabecular bone. The micro-voxel structure of spongiosa requests a voxel structure also for the phantom as a whole. Part II of this study will provide extensive information on this issue. Therefore, for the purposes of dosimetry, the mesh phantoms FASH and MASH were converted to voxelized phantoms, which, depending on the voxel resolution, will reduce the smoothness of all mesh surfaces. The FAX06 and the MAX06 phantoms have a cubic voxel resolution of 1.2 mm. The same voxel resolution was planned for the new FASH and MASH phantoms.

Binvox, the software used for the voxelization of the FASH and the MASH phantoms, can process up to 1024 voxels per matrix dimension and the computer used for the phantom construction can handle up to 750 voxels per matrix dimension. Consequently, it was not possible to voxelize the mesh phantoms as a whole with a 1.2 mm cubic voxel resolution in one Binvox execution process. In order to maintain a certain smoothness of all surfaces, the voxelization was done in steps:

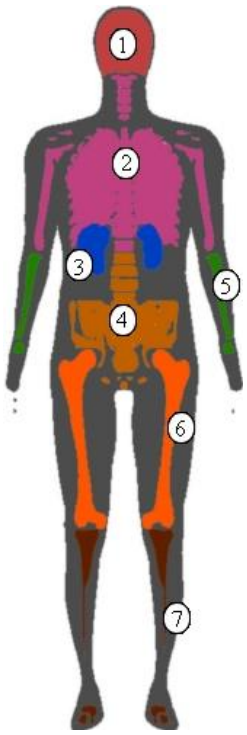

Figure 12. Regions for the voxelization

1) Organs and bones were voxelized separately in seven regions according to figure 12. Regions 1 to 4 correspond to the regions described in sections 2.3.3.1 – 2.3.3.4, while regions 5 to 7 represent the lower arm bones and the upper and lower leg bones.

2) Using the ImageJ software, which allows for 3D visualization of stacks of images, the voxelized organ volumes were adjusted and fitted into their locations within the phantom.

3) Next, the phantom's surface, spinal cord, lymphatic nodes, muscle tissue, connective tissue and cartilage were voxelized.

4) The first voxel at any point on the surface was defined as a skin voxel, except for the region of the eyes.

5) In the voxelized phantoms, general soft tissue was segmented around the muscle tissue and some organs to account for muscular fascia, tendons, blood and blood vessels. These tissues were not explicitly segmented because they are not relevant for the calculation of the effective dose (ICRP 2007), but can be modelled in the future if necessary.

6) After segmentation and volume adjustment of all organs, skin, muscle and general soft tissue, the remaining volume was defined as adipose tissue, i.e. subcutaneous adipose between skin and muscle tissue as well as visceral adipose around internal organs

Finally, segmentation of the bone tissues as well as contents inside walled organs, like stomach, colon, small intestine, gall bladder and urinary bladder was done using in-house software. The skeletons were segmented into cortical bone, spongiosa and medullary yellow bone marrow (YBM) based on skeletal tissue volumes, which have been calculated using data from tables 9.1, 9.3 and 9.4 of ICRP89 (ICRP 2002) and table 41 of ICRP70 (ICRP 1995) and by applying to them a method introduced earlier (Kramer et al 2006a). The calculated ICRP-based skeletal tissue volumes will be presented in the next chapter together with the skeletal tissue volumes, which have actually been segmented in the voxelized FASH and the MASH skeletons.

3. Results

3.1 Body surface

Figures 13 to 16 show the 3D surfaces of the FAX06 and the MAX06 voxel phantoms, the FASH and the MASH mesh phantoms and the FASH and the MASH voxelized phantoms. Compared to the natural bodies of the mesh phantoms, now FAX06 and MAX06 appear only as primitive mock-ups of humans. No ears, poorly modelled faces and female breasts, and exaggerated trunks and shoulders are some of the shortcomings of the previous voxel phantoms which catch the eye. Although the voxelization of the mesh phantoms reduces the smoothness of the body surface, the figures show that improved small structures, like ears, noses, lips, etc., of the mesh phantoms are maintained also in the voxelized versions.

This study is not just about improving the appearance of the body surface, because for exposure from external radiation the shape of the body, i.e. the distribution of muscle and adipose, can have a significant influence on organ and tissue absorbed dose, which will be shown in part II of this study. Especially the lateral views shown in figures 14 and 16 show a thinner diameter of the previous voxel phantoms compared to the mesh phantoms. It seems that a supine position of a scanned individual not only causes internal organs to move towards the thorax, but also causes abdominal adipose being gravitationally shifted sideward, thereby reducing the diameter in sagittal direction.

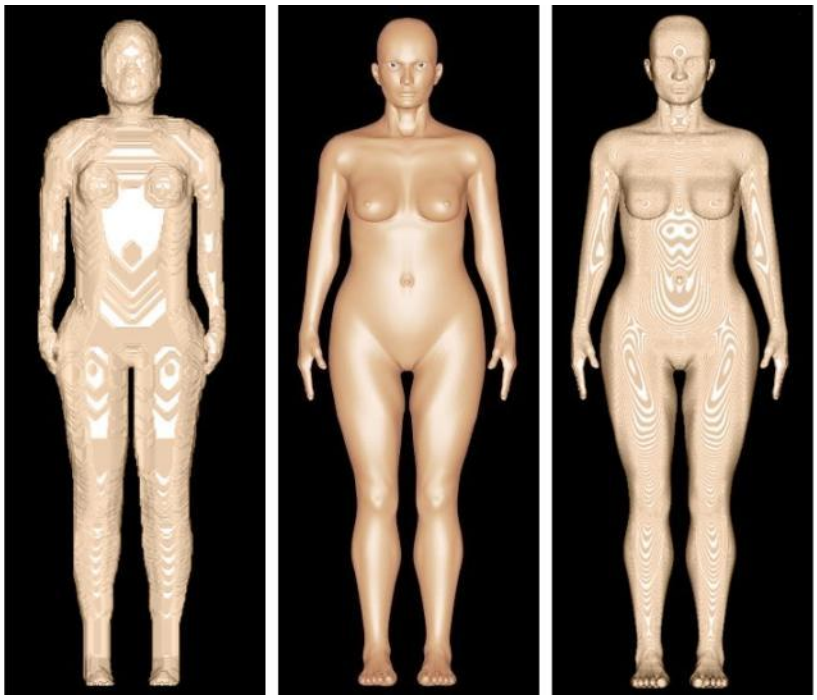

Figure 13. Frontal view of the surfaces of the phantoms FAX06 voxel (left), FASH mesh (center) and FASH voxelized (right)

Figure 14. Lateral view of the surfaces of the phantoms FAX06 voxel (left), FASH mesh (center) and FASH voxelized (right)

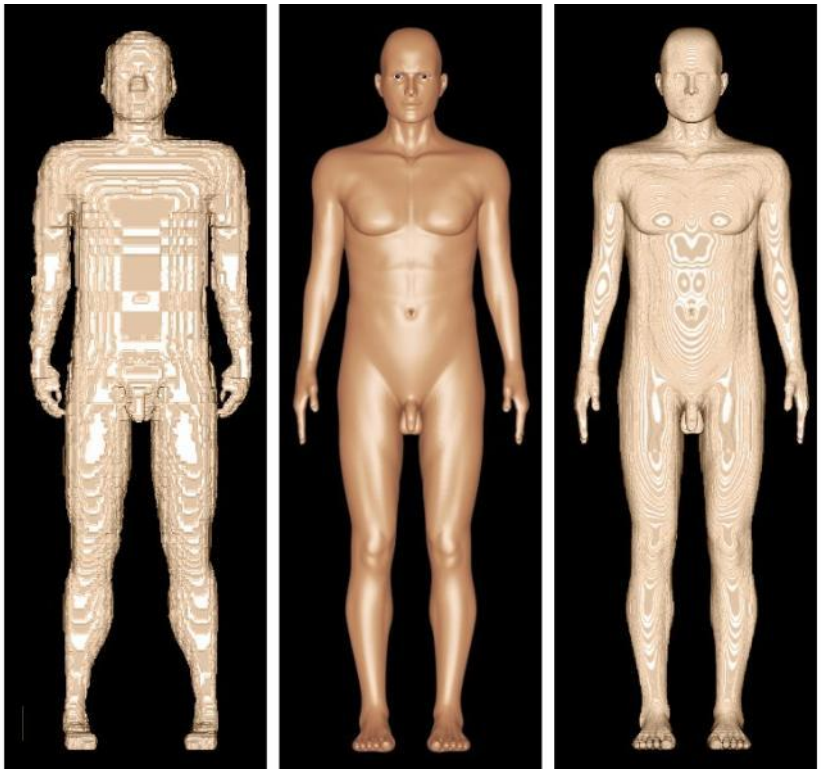

Figure 15. Frontal view of the surfaces of the phantoms MAX06 voxel (left), MASH mesh (center) and MASH voxelized (right)

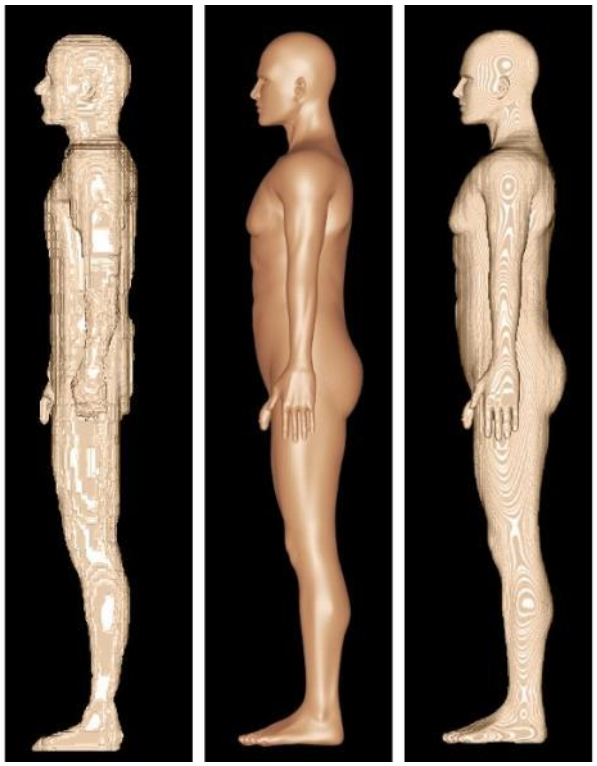

Figure 16. Lateral view of the surfaces of the phantoms MAX06 voxel (left), MASH mesh (center) and MASH voxelized (right)

3.2 Skeleton

Figures 17 to 20 show the skeletons of the FAX06 and the MAX06 voxel phantoms, of the FASH and the MASH mesh phantoms and of the FASH and the MASH voxelized phantoms. The shortcomings of the previous skeletons are obvious: The pelvises are too small and are the same for the male and the female phantom; the cervical vertebrae are too thick; parts of the spines, the ribs, the sternum and the hand bones have not been segmented; the mandibles are too small. Again one can see that that the cubic voxel resolution of 1.2 mm is sufficient to preserve all necessary details of the bones also in the voxelized versions of the mesh skeletons. The voxelized FASH and MASH skeletons have been segmented into cortical bone and spongiosa, shown in figure 21, and additionally into medullary YBM in the arm and legs bones to allow for skeletal dosimetry based on μCT images of trabecular bone introduced earlier (Kramer et al 2006b, 2007, 2009a, b, Walters et al 2009).

The segmentation of skeletal tissues was based on data from ICRP70 (1996) and ICRP89 (2002) and on a method for the calculation of the ICRP-based skeletal tissue volumes used and described already for the FAX06 and the MAX06 phantoms (Kramer et al 2006a), except for the number of bone sites, which was now increased from nine to eighteen. Tables 2 and 3 show the ICRP-based volumes for cortical bone, spongiosa and medullary YBM together with the volumes actually segmented in the skeletons of the FASH and the MASH voxelized phantoms. The bold, italic numbers represent the volumes which deviate from the theoretical ICRP-based value by more than 10%. These are for cortical bone the ribs and all vertebrae and for spongiosa the ribs and the cervical vertebrae in case of the FASH voxelized phantom. For the MASH voxelized phantom one finds for cortical bone also the ribs and all vertebrae but for spongiosa cervical and thoracic vertebrae.

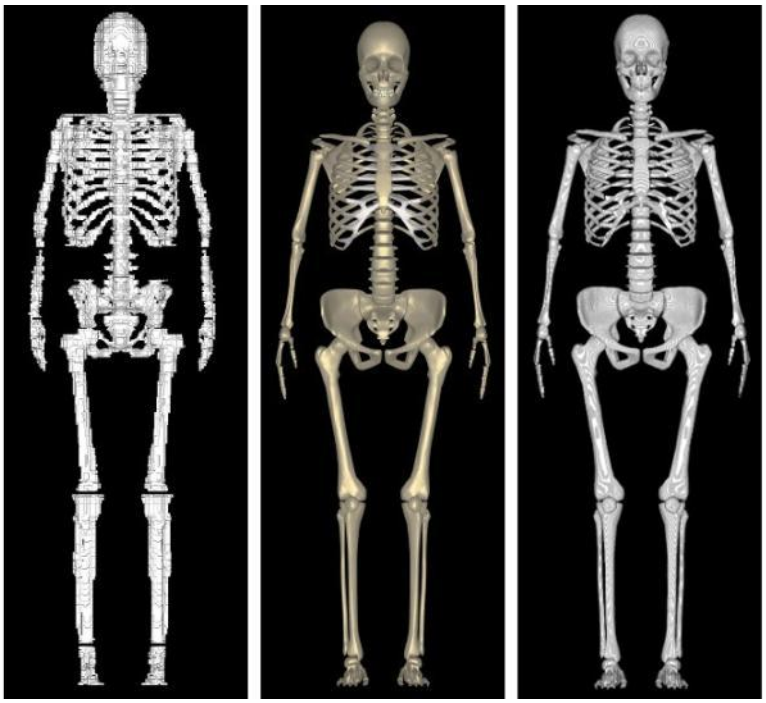

Figure 17. Frontal view of the skeletons of the phantoms FAX06 voxel (left), FASH mesh (center) and FASH voxelized (right)

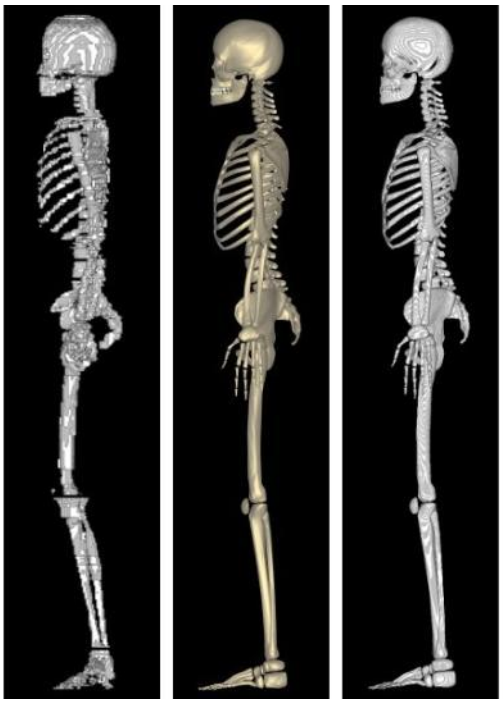

Figure 18. Lateral view of the skeletons of the phantoms FAX06 voxel (left), FASH mesh (center) and FASH voxelized (right)

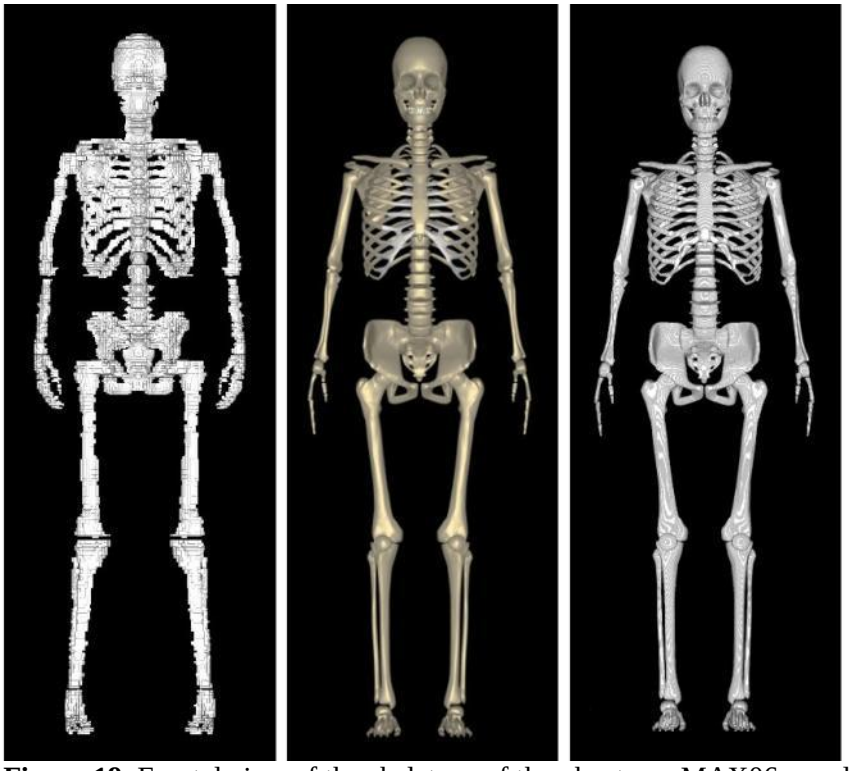

Figure 19. Frontal view of the skeletons of the phantoms MAX06 voxel (left), MASH mesh (center) and MASH voxelized (right)

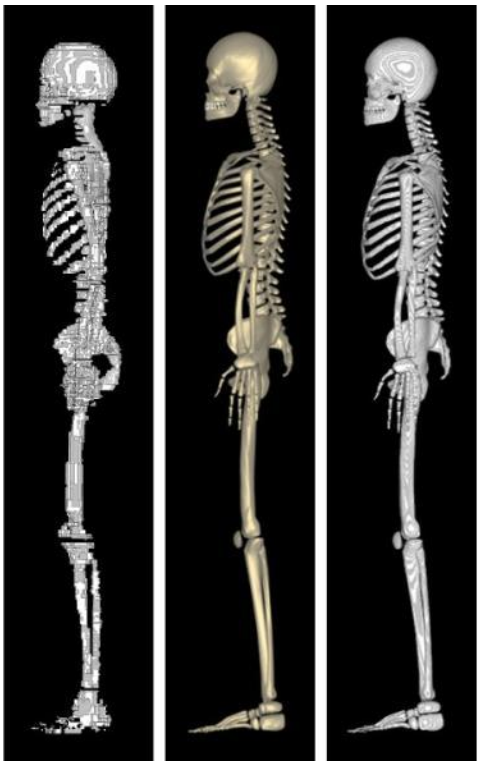

Figure 20. Latertal view of the skeletons of the phantoms MAX06 voxel (left), MASH mesh (center) and MASH voxelized (right)

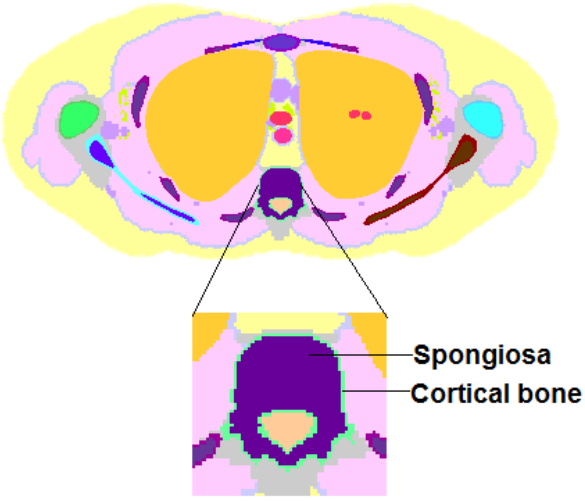

Figure 21. MASH voxelized phantom: Segmentation of spongiosa and cortical bone

The limiting criterion for spongiosa segmentation is that the cortical bone layer surrounding the spongiosa has to consist at least of one voxel layer in order to avoid "holes" in cortical bone. Based on this criterion it was already shown for the segmentation of the FAX06 and the MAX06 skeletons that close agreement with ICRP-based theoretical skeletal tissue volumes is not always possible, especially for the ribs and the spine. The segmentation of the voxelized FASH and MASH skeletons confirms these earlier findings and meanwhile others made similar experiences (Zankl et al 2007).

Table 2. Female theoretical and really segmented skeletal tissue volumes

	ICRP-based	FASH	ICRP-based	FASH	ICRP-based	FASH
Skeletal region	Cortical bone (cm^3)	Cortical bone (cm^3)	Spongiosa (cm^3)	Spongiosa (cm^3)	Medullary YBM (cm^3)	Medullary YBM (cm^3)
Hands	61.1	61.1	41.3	41.6		
Radii and Ulnae	56.8	57.6	60.0	59.3	38.4	38.4
Humeri	51.2	51.7	150.3	150.1	57.6	57.4
Ribs	83.9	***139.9***	206.3	***154.9***		
Sternum	20.1	19.9	40.0	41.4		
Scapulae	63.6	65.8	68.5	70.8		
Clavicles	12.7	12.6	22.0	22.2		
Cervical vertebrae	19.7	***26.3***	107.9	***65.8***		
Thoracic vertebrae	38.9	***75.0***	317.7	293.8		
Lumbar vertebrae	47.2	***63.5***	245.2	259.8		
Sacrum	45.3	45.4	138.7	139.9		
Skull	308.3	311.7	191.0	191.6		
Mandible	30.7	31.8	20.0	20.0		
Pelvis	180.1	185.2	338.5	350.1		
Femora	156.8	154.0	505.1	518.9	198.3	198.7
Patellae	11.7	11.6	14.5	14.6		
Tibiae and fibulae	198.0	195.8	230.5	230.1	132.2	132.2
Feet	181.8	180.4	99.8	100.0		
Total volume	1567.8	1689.3	2797.5	2724.9	426.5	426.7

Table 3. Male theoretical and really segmented skeletal tissue volumes

	ICRP-based	MASH	ICRP-based	MASH	ICRP-based	MASH
Skeletal region	Cortical bone (cm**3)	Cortical bone (cm**3)	Spongiosa (cm**3)	Spongiosa (cm**3)	Medullary YBM (cm**3)	Medullary YBM (cm**3)
Hands	79.7	78.9	54.7	54.9		
Radii and Ulnae	86.5	86.4	93.8	94.5	59.0	59.1
Humeri	86.0	85.7	214.7	216.0	89.9	89.8
Ribs	183.9	***204.7***	273.0	260.2		
Sternum	28.8	28.8	52.2	52.3		
Scapulae	120.4	120.2	91.4	91.5		
Clavicles	22.4	22.4	29.0	29.2		
Cervical vertebrae	23.9	***51.5***	134.8	***103.3***		
Thoracic vertebrae	47.7	***120.2***	404.5	***338.7***		
Lumbar vertebrae	58.1	***81.7***	312.5	292.7		
Sacrum	65.1	64.9	182.3	182.1		
Skull	422.2	417.6	249.4	250.4		
Mandible	42.5	42.0	26.2	25.8		
Pelvis	259.9	257.9	443.1	443.1		
Femora	197.7	199.7	667.1	667.5	277.4	277.1
Patellae	19.1	19.0	22.0	22.0		
Tibiae and fibulae	241.0	245.7	321.5	321.2	184.8	184.0
Feet	221.3	219.4	143.9	145.3		
Total volume	2206.0	2346.7	3715.9	3590.7	611.1	610.0

The percentage differences between the actually segmented volumes and the ICRP-based volumes for total cortical bone are +6.4% (+8.6%) for the MASH phantom and +7.7% (+17.1%) for the FASH phantom, and for total spongiosa -3.4% (-4.9%) for the MASH phantom and -2.6% (-9.3%) for the FASH phantom. The percentages in brackets refer to the MAX06 and the FAX06 phantoms, respectively, and one can see that at least it was possible to reduce the earlier differences with the mesh-based skeletons.

3.3 Organs and tissues

According to the methodology outlined in the previous chapter, all organs and tissues mentioned in table 1 have been designed based on polygon mesh surfaces and then voxelized observing the reference masses given by ICRP89 (2002) as closely as possible. The tissue densities used during this process were taken from or based on ICRU 44 and 46 (ICRU 1989, 1992), like in earlier studies (Kramer et al 2006a). Figures 22a and 22b show most of the soft tissue organs the way they were assembled inside the body as mesh and as voxelized version, for the FASH and the MASH phantoms, respectively. These comparative presentations of the two versions demonstrate again that 1.2 mm cubic voxels are small enough to maintain all important anatomical properties of the mesh phantoms also in the voxelized phantoms.

Tables 4 and 5 show the organ and tissue masses for the voxelized FASH and MASH phantoms, respectively, together with the reference masses as given by ICRP89 (ICRP 2002) and with the corresponding masses of the FAX06 and the MAX06 phantoms. The last columns of the tables contain the percentage differences between organ and tissue masses of the FASH and the MASH phantoms and the ICRP89 data. For all organs and tissues relevant for the calculation of the effective dose, mass

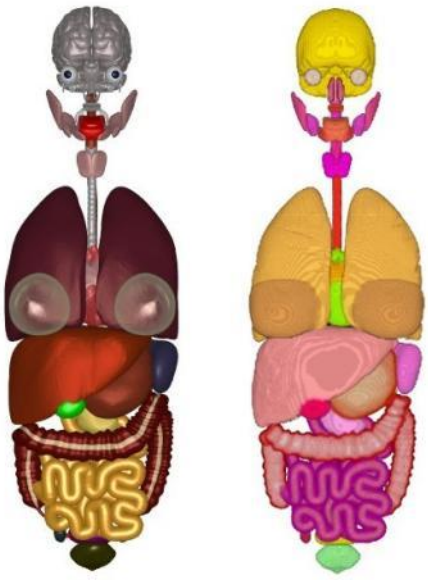

Figure 22a. Female organs: mesh (left) voxelized (right)

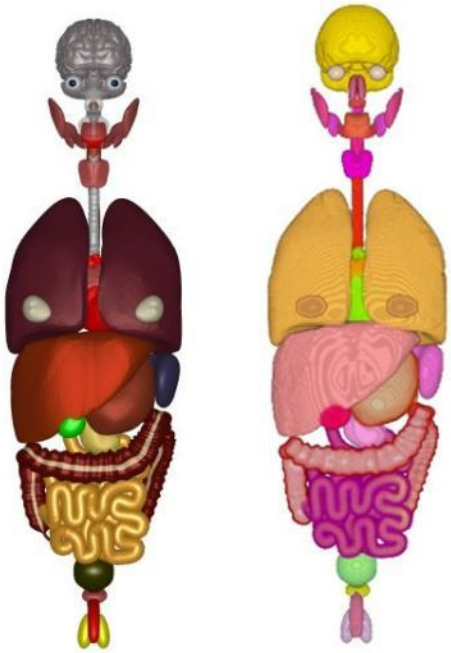

Figure 22b. Male organs: mesh (left) voxelized (right)

Table 4. Female organ / tissue masses from ICRP 89, for the FAX06 and the FASH voxelized phantoms

FEMALE ADULT ORGAN / TISSUE	ICRP89 [g]	FAX06 [g]	FASH [g]	FASH / ICRP89 [%]
Adrenals	13.0	13.0	13.3	2.3
Salivary Glands	70.0	70.0	69.2	-1.1
Oesophagus	35.0	35.0	34.3	-2.0
Stomach wall	140.0	140.0	140.0	
Small Intestine wall	600.0	600.0	599.3	-0.1
Colon wall	360.0	360.0	355.7	-1.2
Liver	1400.0	1400.0	1400.0	
Gallblader wall	8.0	8.0	8.2	2.5
Pancreas	120.0	120.0	118.8	-1.0
Brain	1300.0	1300.0	1283.6	-1.3
Breasts	500.0	500.0	501.0	0.2
Heart wall	250.0	250.0	252.2	0.9
Adipose	19000.0	18000.0	19053.4	0.3
Skin	2300.0	2300.0	2303.4	0.1
Muscle	17500.0	17497.9	17493.4	-0.04
Lungs	950.0	950.0	946.6	-0.4
Skeleton	7800.0	7355.5	7343.4	-5.9
Spleen	130.0	130.0	130.0	
Thymus	20.0	20.0	20.0	
Thyroid	17.0	17.0	16.8	-1.2
Kidneys	275.0	275.0	275.0	
Bladder wall	40.0	40.0	39.7	-0.8
Ovaries	11.0	11.0	11.0	
Uterus	80.0	80.0	80.0	
	52919.0	51472.4	52488.3	-0.8
Tongue	60.0		73.0	21.7
Larynx	19.0			
Extra thorarcic airw.		112.6	94.1	
GI contents	830.0	830.0	710.0	-14.5
Gall bladder cont.	48.0	48.0	41.2	-14.2
Trachea	8.0	8.1	8.6	7.5
Tonsils	3.0			
Ureter/Urethra	18.0			
Fallopian Tubes	2.1			
Pituary Gland	0.6			
Eyes	15.0	15.0	16.5	9.3
Optic nerve		1.3		
Blood	3570*			
Hard palate		30.0		
Feces		33.6		
Spinal chord		72.2	70.9	
	57492.7	52623.3	53502.6	-7.0
Connective Tissue	2100.0	2100.0		
Lymphatic Nodes	600.0	300.0	298.7	-50.2
	60192.7	55023.2	53801.3	-10.6
Soft tissue		3979.8**	6295.7***	
Total mass	60192.7	59003.0	60097.0	-0.2
Height	163 cm	163.1 cm	162.5 cm	-0.3

*without lungs, **includes blood, ***includes blood and connective tissue

Table 5. Male organ / tissue masses from ICRP 89, for the MAX06 and the MASH voxelized phantoms

MALE ADULT ORGAN / TISSUE	ICRP89 [g]	MAX06 [g]	MASH [g]	MASH / ICRP89 [%]
Adrenals	14.0	14.0	14.0	
Salivary Glands	85.0	85.0	83.7	-1.5
Oesophagus	40.0	40.0	45.2	0.4
Stomach wall	150.0	150.0	148.5	-1.0
Small Intestine wall	650.0	650.0	652.8	0.4
Colon wall	370.0	370.0	366.7	-0.9
Liver	1800.0	1800.0	1800.0	
Gallbladder wall	10.0	10.0	10.0	
Pancreas	140.0	140.0	140.0	
Brain	1450.0	1450.0	1438.2	-0.8
Heart wall	330.0	330.0	332.0	0.6
Adipose	14500.0	14544.1	14565.6	0.5
Skin	3300.0	3383.9	3311.9	0.4
Muscle	29000.0	29000.0	29001.1	
Lungs	1200.0	1200.0	1181.5	-1.5
Skeleton	10500.0	9950.4	9894.9	-5.8
Spleen	150.0	150.0	150.0	
Thymus	25.0	25.0	24.8	-0.8
Thyroid	20.0	20.0	20.1	0.5
Kidneys	310.0	310.0	310.0	
Bladder wall	50.0	50.0	50.0	
Testes	35.0	35.0	35.2	0.6
Prostate	17.0	17.0	17.1	0.6
	64146.0	63724.4	63593.3	-0.9
Breasts	25.0		24.7	-1.2
Tongue	73.0		39.4	-46.0
Larynx	28.0			
Extra thorarcic airw.		133.4	121.2	
GI contents	900.0	900.0	964.4	7.2
Gall bladder cont.	58.0	58.0	55.8	-3.8
Trachea	10.0	10.3	12.8	
Tonsils	3.0			
Ureter/Urethra	26.0			
Epididymes	4.0			
Pituary Gland	0.6			
Eyes	15.0	15.1	16.2	8.0
Optic nerve		1.6		
Blood	4900*			
Hard palate		33.6		
Feces		39.2		
Spinal chord		183.8	113.7	
	70188.6	65099.4	64941.5	-7.5
Connective Tissue	2600.0	2600.0		
Lymphatic Nodes	730.0	365.0	350.0	-52.1
	73518.6	68064.4	65291.5	-11.2
Soft tissue		4426.3**	7491.9***	
Total mass	73518.6	72490.7	72783.4	-1.0
Height	176 cm	175.3 cm	175.6 cm	-0.2

*without lungs, **includes blood, ***includes blood and connective tissue

differences are smaller than 2.6%, with two exceptions: the masses of the skeleton and of the lymphatic nodes. The skeleton mass differences are almost 6%, because the ICRP89 total skeleton mass contains a certain amount of cartilage, which actually is not located in the skeleton (ears, nose, etc.). This "off" skeleton part of cartilage, assumed to be 50% of the total cartilage mass, was not segmented in the voxelized FASH and the MASH phantoms and is therefore also not included in the total skeleton mass. If one would reduce the ICRP89 total skeleton mass by 50% of the cartilage mass, the percentage skeletal mass differences would become -0.1% for the FASH phantom and 0.4% for the MASH phantom. Similar considerations apply to the mass of the lymphatic nodes, a part of which is located in the bone marrow. Only about 50% of the ICRP89 mass for the lymphatic nodes was segmented in the two phantoms. These procedures have already been applied to the segmentation of the FAX06 and the MAX06 phantoms. Tables 4 and 5 show that with respect to total body weights and heights, agreements between the ICRP89 data and the FASH and MASH phantom data are 1% or less.

Sato et al (2007b) reported on the development of a CT-based male voxel phantom in upright posture. They found, that kidneys, liver, pancreas and stomach in the upright standing phantom had moved 1-2 cm towards the feet compared to their positions in the voxel phantom based on the supine position of the same scanned individual. In this study it was found that in the MASH phantom kidneys, liver, pancreas and stomach are located 2.8, 2.5, 4.7 and 3.1 cm, respectively, closer toward the feet compared to their positions in the MAX06 phantom. Such differences of organ positions can have a significant impact on organ equivalent doses, for example, in X-ray diagnosis for organs located close to the edges of the radiation field.

3.4 Comparison with other mesh-based phantoms

In 2007, a human phantom, entirely based on polygon mesh surfaces, was presented by Santos and Frère (2007a, b) at two conferences. Using images of a human skeleton and anatomical atlases, the authors applied the Blender software (Blender 2009) to create the surface, the skeleton and general soft tissue of a male body with the "box modelling" tool. Their results show "proportional", "athletic" and "obese" versions of the phantom in order to demonstrate how easy one can change body dimensions of mesh-based phantoms. Information about the origin of the phantom's surface was not given in these presentations and human organs have not been modelled. The use of the Blender software represents the only point of contact with the FASH and the MASH phantoms, because materials, methods and results of two studies are quite different.

Comparison between the FASH and the MASH phantoms and the RPI_AM and the RPI_AF phantoms (Zhang et al 2009), mentioned in the introduction, will be made for the anatomical part, while part II of this study will compare dosimetric results. Common ground one can find in the fact that all four phantoms, FASH/MASH and RPI_AF/RPI_AM, have organ and tissue masses adjusted to ICRP89 data. Beyond that, the two pairs of phantoms differ with respect to the raw material used, to the 3D modelling process and the software applied, to the created anatomy and to the step in the process at which the adjustment of organ volume was made.

For the RPI phantoms, 140 organs and anatomical structures have been downloaded from www.anatomium.com. After repair of open meshes, deformation and volume adjustment were made using MATLAB ^{R} 7.4. Then the phantoms were voxelized using in-house voxelization software. For the development of the FASH and MASH phantoms, a skeleton and eight organs were downloaded from the internet. All other organs were 3D modelled based on anatomical atlases. MakeHuman (MakeHuman 2009) and Blender (Blender 2009) were used to create the mesh phantoms. Binvox (Min 2009,

Nooruddin and Turk 2003) and ImageJ (ImageJ 2009) were used to voxelize the mesh phantoms and to adjust organ and tissue volumes.

The adjustment of organ and tissue volumes based on ICRP89 (ICRP 2002) was done for the FASH and the MASH phantoms after the voxelization, whereas for the RPI_AM and RPI_AF phantoms before the voxelization. Due to the partial volume effect one can expect that organ and tissue volumes would change during voxelization, i.e. that strictly spoken the organ and tissue masses of the voxelized RPI_AM and RPI_AF phantom are not exactly known. The cubic voxel sizes of the RPI_AM and the RPI_AF phantoms are 3.0 mm and 2.5 mm, respectively, i.e. perhaps the effect of the partial volume effect on the organ masses is small. Table 3 of the paper by Zhang et al (2009) contains organ and tissue masses for the RPI_AM and RPI_AF mesh phantoms, whereas tables 4 and 5 of this study contain organ and tissue masses for the voxelized FASH and MASH phantoms.

In the paper of Zhang et al (2009), figure 5 shows the bodies of the RPI_AM and the RPI_AF phantoms. The female phantom has a male body shape because it seems to be a scaled down version of the male phantom. The female pelvis is smaller than the male pelvis. Usually women have a larger pelvis than men for obvious reasons. Both RPI phantoms show interruptions of the frontal ribs. FASH and MASH, on the other hand, have female and male bodies, respectively, showing the typical differences with respect to body shape, the size of the pelvis and to the fat and muscle distribution usually found between women and men.

In Zhang et al's paper, figures 8a, 9a, 10a and 11a show body cross-sections of the RPI_AM phantom for the urinary bladder, the testes, the liver and the lungs, respectively, and figures 12a and 13a of the RPI_AF phantom for the ovaries and the breasts, respectively. The male organ locations are similar to those found in the MASH phantoms, except for the urinary bladder and the testes. In the MASH phantom, the urinary bladder is partly located behind the pubis, a bone of the pelvis, and the testes are located outside the trunk between the legs. From figure 8a of the paper of Zhang et al (2009) it seems that no bone structure is located in front of the bladder and the RPI_AM testes in figure 9a are located inside the lower abdomen. Liver and lungs have similar positions in both male phantoms and the ovaries in both female phantoms. Female breasts have been modelled differently in the FASH and the RPI_AF phantoms. Similar to the REGINA phantom, the FASH breasts consist of homogeneous soft tissue, whereas in the RPI_AF breasts, glandular tissue and adipose have been modelled separately.

Although pursuing the same objective, the paper of Zhang et al (2009) and this study use different materials, software and concepts. The resulting phantoms are anatomically not similar, which will also be reflected in the differences between dosimetric results found in part II for the FASH and the MASH phantoms on the one hand, and the RPI_AF and RPI_AM phantoms on the other hand.

4. Conclusion

Human computational phantom development for radiation protection, radiology and nuclear medicine has come a long way from the early homogeneous 30 cm slab phantoms to the anatomical models created with tools of computer graphics and animated film. FASH and MASH are ICRP89-based female and male adult human phantoms designed using polygon mesh surfaces, independent from digital images of a specific human individual. Positioning of organs and tissues corresponds to adult persons in standing posture. The mesh-based phantoms represent improved human anatomy compared to their predecessors FAX06 and MAX06. The FASH and MASH phantoms are mesh models like the RPI_AF and RPI_AM phantoms, but they are based on different anatomical 3D surfaces and developed with different 3D modelling and voxelization software. Anatomically, FASH and MASH differ significantly from RPI_AF

and RPI_AM. The implications of these differences will be discussed in part II of this study, which will compare dosimetric results with corresponding data published for other phantoms.

In particular, this paper has shown that it is possible

a) to develop ICRP-based human phantoms using only modern software tools freely available on the internet and anatomical atlases, which may also encourage investigators to build their own phantoms, who usually have no or limited access to medical images,

b) to make whole-body CT scanning of individuals, especially of volunteers, unnecessary in order to receive anatomical images just for phantom design, which does not diminish the importance of acquiring medical images for patient-specific applications, radiation therapy, for example,

c) to improve significantly the representation of the human anatomy, particularly of complex walled organs, like the colon and the small intestine and

d) to easily modify the human body in the future to create phantoms with different weights and heights or postures.

In the future, FASH and MASH will be the base models for the 32 phantoms mentioned in section 1.3, i.e. that the two phantoms will be modified with respect to weight and height in order to allow for the calculation of patient-specific conversion coefficients for adults submitted to examinations in X-ray diagnosis. The conversion coefficients will be introduced into the CALDose_X software to broaden its application in the world of real patients. Like their predecessors FAX06 and MAX06, FASH and MASH will eventually be made available to the scientific community.

5. Acknowledgement

The authors would like to thank the Conselho Nacional de Desenvolvimento Científico e Tecnológico - CNPq and the Fundação de Amparo à Ciência do Estado de Pernambuco - FACEPE for financial support.

6. References

Alsmiller R G Jr. and Moran H S 1968 Dose rate from high-energy electrons and photons *Nucl. Instr. Meth.* ***58****,343-344*

Alsmiller R G Jr, Armstrong T W and Coleman W A 1970 The absorbed dose and dose equivalent from neutrons in the energy range 60 to 3000 MeV and protons in the energy range 400 to 3000 MeV *Report ORNL-TM-2924 (rev.),Oak Ridge National Laboratory, Oak Ridge, Tenn., USA*

Artist-3D 2009 http://artist-3d.com/free_3d_models/dnm/model_disp.php?uid=568&ad=02anatomy_design.php&count=count Last access June 2009

Auxier J A, Snyder W S and Jones T D 1969 Neutron interactions and penetration in tissue *In: Attix F H and Roesch W C (eds.) Radiation dosimetry, 2nd ed.,Vol.1, pp.275-316, New York, Academic Press*

Badal A, Kyprianou I, Badano A and Sempau J 2008 Monte Carlo simulation of a realistic anatomical phantom described by triangle meshes: Application to prostate brachytherapy imaging, Radiotherapy and Oncology 86, 99-103

Beck H L 1970 A new calculation of dose rates from high energy electrons and photons incident on 30 cm water slabs *Nucl. Instr. Meth.* ***78*** *333-334*

Blender 2009 http://www.blender.org/ Last access June 2009

Caon M Bibbo G and Pattison J 1999 An EGS4-ready tomographic computational model of a fourteen-year-old female torso for calculating organ doses from CT examinations *Phys. Med. Biol.* ***44*** *2213-2225*

Cristy M 1980 Mathematical phantoms representing children at various ages for use in estimates of internal dose *Report ORNL/NUREG/TM-367, Oak Ridge National Laboratory, Oak Ridge, Tenn., USA*

Dawson T W Caputa K and Stuchly M A 1997 A comparison of 60 Hz uniform magnetic and electric induction in the human body *Phys. Med. Biol.* ***42*** *2319-2329*

Dimbylow P J 1995 The development of realistic voxel phantoms for electromagnetic field dosimetry *In: Proceedings of an International Workshop on Voxel Phantom Development held at the National Radiological Protection Board, Chilton, UK, 6-7 July*

Dimbylow P J 2005 Development of a female voxel phantom, NAOMI, and its application to calculations of induced current densities and electric fields from applied low frequency magnetic and electric fields *Phys. Med. Biol.* ***50*** *1047-1070*

Ferrari P and Gualdrini G 2005 An improved MCNP version of the NORMAN voxel phantom for dosimetry studies *Phys. Med. Biol.* ***50*** *4299-4316*

Fill U A, Zankl M, Petoussi-Henss N, Siebert M and Regulla D 2004 Adult femaale voxel models of different stature and photon conversion coefficients for radiation protection *Health Phys.* ***86*** *253-272*

Free 3D Models 2009 http://gfx-3d-model.blogspot.com/2008/09/skeleton-3d-model.html Last access June 25 2009

Gibbs S J, Pujol A, Chen T S, Malcolm A W and James A E 1984 Patient risk from interproximal radiography *Oral Surg. Oral Med. Oral Pathol.,* ***58,*** *347-354*

Heart 3dxtras 2009 http://www.3dxtras.com/3dxtras-free-3d-models-details.asp?prodid=37 Last access June 2009

Heart model 2009 Project MedX, Heart model with Valves http://ccvweb.csres.utexas.edu/ccv/projects/medx/heart/index.php Last access June 2009

ICRP 1995 Basic Anatomical and Physiological Data for use in Radiological Protection: The Skeleton. *ICRP Publication 70* (Oxford: Pergamon)

ICRP 1996 Conversion Coefficients for use in Radiological Protection against External Radiation. ICRP Publication 74 *International Commission on Radiological Protection, Pergamon Press, Oxford*

ICRP 2002 Basic Anatomical and Physiological Data for Use in Radiological Protection: Reference Values *ICRP Publication 89* (Oxford: Pergamon)

ICRP 2007 Recommendations of the International Commission on Radiological Protection *ICRP Publication 103 Ann. ICRP 37 (2-3) Elsevier Science Ltd., Oxford*

ICRP 2009 The ICRP Reference Computational Phantoms for the Adult Male and Female *ICRP Publication 110* (Oxford: Pergamon)

ICRU 1989 Tissue Substitutes in Radiation Dosimetry and Measurement *ICRU Report No. 44* International Commission On Radiation Units And Measurements, Bethesda, MD, USA

ICRU 1992 Photon, Electron, Proton and Neutron Interaction Data for Body Tissues *ICRU Report No. 46* International Commission On Radiation Units And Measurements, Bethesda, MD, USA

ImageJ 2009 National Institute of Health. ImageJ: Image Processing and Analysis in Java http://rsbweb.nih.gov/ij/index.html Last access June 2009

Inria_stomach 2009 http://www-c.inria.fr/gamma/download/affichage.php?dir=ANATOMY &name=Stomach Last access June 2009
Inria_Y5733 2009 http://www-c.inria.fr/gamma/download/affichage.php?dir=ANATOMY &name =Y5733_KIDNEY Last access June 2009
Inria_Y5820 2009 http://www-c.inria.fr/gamma/download/affichage.php?dir=ANATOMY &name =Y5820_LIVER Last access June 2009
Inria_Y6003 2009 http://www-c.inria.fr/gamma/download/affichage.php?dir=ANATOMY &name =Y6003_ovaries Last access June 2009
Inria_Y6396 2009 http://www-c.inria.fr/gamma/download/affichage.php?dir=ANATOMY &name =Y6396_spine Last access June 2009
Irving D D, Alsmiller R G Jr. and Moran H S 1967 Tissue current-to dose conversion factors for neutrons with energies from 0.5 to 60 MeV *Report ORNL-4032, Oak Ridge National Laboratory, Oak Ridge, Tenn., USA*
Jeong J H, Cho S, Lee C, Cho K and Kim C 2008 Development of deformable computational model from Korean adult male based on polygon and NURBS surfaces *11th International Conference on Radiation Shielding, 13-18 April 2008, Callaway Gardens, Pine Mountain, Georgia, USA*
Johnson P, Lee C, Johnson K, Siragusa D and Bolch W 2009 The influence of patient size on dose conversion coefficients: a hybrid phantom study for adult cardiac catheterization *Phys. Med. Biol.* ***54*** *3613-3629*
Jones D G 1997 A Realistic Anthropomorphic Phantom For Calculating Organ Doses Arising From External Photon Irradiation. *Rad. Prot. Dos.* ***72****, No.1, pp.21-29*
Kawrakow I and Rogers D.W.O. 2003 The EGSnrc code system: Monte Carlo simulation of electron and photon transport, *NRC Report PIRS-701*
Kramer R, Zankl M, Williams G, Drexler G 1982 The Calculation of Dose from External Photon Exposures Using Reference Human Phantoms and Monte Carlo Methods. Part I: The Male (ADAM) and Female (EVA) Adult Mathematical Phantoms *GSF-Report S-885.Reprint July 1999.Institut fuer Strahlenschutz, GSF-Forschungszentrum fuer Umwelt und Gesundheit, Neuherberg-Muenchen*
Kramer R, Vieira J W, Khoury H J, Lima F R A and Fuelle D 2003 All About MAX: a Male Adult voXel Phantom for Monte Carlo Calculations in Radiation Protection Dosimetry *Phys. Med. Biol*., **48**, No. 10, 1239-1262
Kramer R, Vieira J W, Khoury H J, Lima F R A, Loureiro E C M, Lima V J M and Hoff G 2004 All about FAX: a Female Adult voXel Phantom for Monte Carlo Calculation in Radiation Protection Dosimetry *Phys. Med. Biol.* **49**, 5203-5216
Kramer R, Khoury H J, Vieira J W and Lima V J M 2006a MAX06 and FAX06: Update of two adult human phantoms for radiation protection dosimetry *Phys. Med. Biol.* **51** 3331-3346
Kramer R, Khoury H J, Vieira J W and Kawrakow I 2006b Skeletal dosimetry in the MAX06 and the FAX06 phantoms for external exposure to photons based on vertebral 3D-microCT images *Phys.Med.Biol.* **51** 6265-6289
Kramer R, Khoury H J, Vieira J W and Kawrakow I 2007 Skeletal dosimetry for external exposure to photons based on μCT images of spongiosa from different bone sites *Phys.Med.Biol.* ***52*** *6697-6716*
Kramer R, Khoury H J and Vieira J W 2008 CALDose_X a software tool for the assessment of organ and tissue doses, effective dose and cancer risk in diagnostic radiology *Phys. Med. Biol.* **53** 6437-6459
Kramer R, Khoury H J, Vieira J W, Robson-Brown K and Fuelle D 2009a Electron absorbed fractions in skeletal soft tissues based on red bone marrow segmentation at runtime in microCT images of human trabecular bone *World Congress 2009 – Medical Physics and Biomedical Engineering, 7-12 September 2009, Munich, Germany.*

Kramer R, Khoury H J, Vieira J W and Robson Brown K A 2009b Skeletal dosimetry for external exposures to photons based on μCT images of spongiosa: Consideration of voxel resolution, cluster size and medullary bone surfaces *Med Phys* (in press)

Lee C and Lee J 2004 Korean adult male voxel model segmented from magnetic resonance images *Med. Phys.* ***31*** *1017-1022*

Lee C, Williams J L, Lee C and Bolch W 2005 The UF series of tomographic computational phantoms of pediatric patients *Med. Phys.* ***32*** *3537-3548*

Lee C, Lodwick D, Hasenauer D, Williams J L, Lee C and Bolch W E 2007a Hybrid computational phantoms of the male and female newborn patient: NURBS-based whole-body models *Phys. Med. Biol .**52** 3309-3333*

Lee C, Lee C, Lodwick D and Bolch W E 2007b NURBS-based 3-D anthropomorphic computational phantoms for radiation protection dosimetry applications. *Rad. Prot. Dos.* **127**, 227-232

Lee C, Lodwick D, Williams J L and Bolch W E 2008 Hybrid computational phantoms of the 15-year male and female adolescent: Applications to CT organ dosimetry for patients of variable morphometry *Med. Phys. **35**(6)2366-2382*

MakeHuman 2009 http://www.makehuman.org/blog/index.php Last access June 2009

Min P 2009 Binvox: 3D mesh voxelizer, http://www.google.com/search?q=binvox Last access June 2009

Na Y H, Zhang J and Xu X G 2008 A Mesh-Based Anatomical Deformation Method for Creating Size-adjustable Whole-body Patient Models. *Med. Phys.*, Vol 35(6), 2665

Nagaoka T, Watanabe S, Sakurai K, Kunieda E, Tali M and Yamanaka Y 2004 Development of realistic high-resolution whole-body models of Japanese adult males and females of average height and weight, and applicatition of models to radio-frequency electromagnetis-field dosimetry *Phys. Med. Biol. **49** 1-15*

Nipper J C, Williams J L and Bolch W E 2002 Creation of two tomographic voxel models of pediatric patients in the first year of life *Phys. Med. Biol. **44** 2213-2225*

Noorudin F and Turk G 2003 Simplification and repair of polygonal models using volumetric techniques *IEEE Trans. Vis. Comput. Graphics **9** 191–205*

Petoussi-Henss N and Zankl M 1998 Voxel Anthropomorphic Models as a Tool for Internal Dosimetry, *Rad. Prot. Dos. Vol.**79**, Nos 1-4, pp. 415-418*

Petoussi-Henss N, Zankl M, Fill U and Regulla D 2002 The GSF family of voxel phantoms *Phys. Med. Biol. **47**, 89-106*

Santos C E and Frère A F 2007a Criação de um fantoma computacional multi-uso baseado em modelagem 3D, XII Congresso Brasileiro de Física Médica, Foz do Iguaçu, June 6-9 (available at http://www.abfm.org.br/c2007/pdf/B_152.pdf)

Santos CE and Frère A F 2007b Desenvolvimento de um novo tipo de fantoma baseado em modelagem 3D, VII Workshop de Informática Médica (WIM 2007), Porto de Galinhas June 25-26 (available at http://www.ime.uerj.br/professores/cecas/AnaisWIM2007/sessao5/4-28371.pdf)

Sato K, Noguchi H, Emoto Koga Y and Saito K 2007a Japanese adult male voxel phantom constructed on the basis of CT-images *Rad. Prot. Dos. **123** 337-344*

Sato K, Noguchi H, Endo A, Emoto, Y, Koga S and Saito K 2007b Development of a voxel phantom of Japanese adult male in upright posture *Rad Prot Dos* **127** 205-208

Saito K, Wittmann A, Koga S, Ida Y, Kamei T, Funabiki J and Zankl M 2001 Construction of a computed tomographic phantom for a Japanese male adult and dose calculation system *Radiat. Environ. Biophys. **40** 69-76*

Segars W P 2001 Development of a new dynamic NURBS-based cardiac-torso (NCAT) phantom, Ph.D. Thesis, University of North Carolina

Sidewell J M, Burlin T E and Wheatley B M 1969 Calculation of the absorbed dose in a phantom from photon fluence and some applications to radiological protection *Br. J. Radiol. **42**, 522-529*

Sidewell J M and Burlin T E 1973 Photon fluence calculations for estimating dose distribution in the thorax *Br. J. Radiol. **46**,360-364*

Sjogreen K, Ljungberg M, Wingardh K, Erlandson K and Strand SE 2001 Registration of emission and transmission whole-body scintillation-camera images *J. Nucl. Med.* ***42*** *1563-1570*

Snyder W S 1950 Calculations for maximum permissible exposure to thermal neutrons *Nucleonics* ***6****, 2, 46-50*

Snyder W S 1965 The variation of Dose in Man from Exposure to a Point Source of Gamma Rays, Congrès international sur la radioprotection dans l'utilisation industrielle des radioéléments, 13-15 December 1965, Le Vesinet, France

Snyder W S, Ford M R, Warner G G and Fisher H C 1968 Estimates of absorbed fractions for monoenergetic photon sources uniformly distributed in various organs of a heterogeneous phantom *MIRD Pamphlet No. 5, Journal of Nuclear Medicine, Supplement 3*

Snyder W S, Ford M R and Warner G G 1978 Estimates of absorbed fractions for monoenergetic photon sources uniformly distributed in various organs of a heterogeneous phantom *MIRD Pamphlet No.5, revised, Society of Nuclear Medicine, New York N. Y.*

Snyder W S 1971 Dose distribution in a cylindrical phantom for neutron energies up to 14 MeV, In: Protection against neutron radiation *NCRP Report No.38, pp.46-84, Washington, D. C., National Council on Radiation Protection and Measurements*

Sobotta 2006 Altas de anatomia humana *22nd edition, Guanabara Koogan, Rio de Janeiro*

Stabin M, Watson E, Cristy M, Ryman J, Eckerman K, Davis J, Marshall D and Gehlen K 1995 Mathematical models and specific absorbed fractions of photon energy in the nonpregnant adult female and at the end of each trimester of pregnancy *Report No. ORNL/TM-12907, Oak Ridge National Laboratory, Oak Ridge, Tenn., USA*

Teeth 3dxtras 2009 http://www.3dxtras.com/3dxtras-free-3d-models-details.asp?prodid=8621 Last access June 2009

Walters B R B, Ding G X, Kramer R and Kawrakow I 2009 Skeletal dosimetry in cone beam computed tomography *Med Phys* ***36*** *(7) 2915-2922*

Wikipaedia 2009 http://en.wikipedia.org/wiki/Polygon_mesh, last access June 2009

Williams G, Zankl M, Abmayr W, Veit R and Drexler G 1986 The calculation of dose from external photon exposures using reference and realistic human phantoms and Monte Carlo methods *Phys. Med. Biol.* ***31,*** *347-354*

Wolf-Heidegger 2006 Atlas de anatomia humana Guanabara *Koogan, Rio de Janeiro*

Xu X G, Chao T C, Bozkurt A 2000 VIP-MAN: An Image-based Whole-body Adult Male Model Constructed From Colour Photographs Of The Visible Human Project For Multi-particle Monte Carlo Calculations *Health Phys.* ***78****(5):476-486*

Xu G, Taranenko V, Zhang J and Shi C 2007 A boundary-representation method for designing whole-body radiation dosimetry models: pregnant females at the end of three gestional periods – RPI-P3, -P6 and P9 *Phys. Med. Biol.* ***52*** *7023-7044*

Xu X G, Zhang J Y and Na Y H 2008 Preliminary Data for Mesh-Based Deformable Phantom Development: Is it Possible to Design Person-Specific Phantoms On-demand. The International Conference on Radiation Shielding-11, April 14-17

Xu X G and Eckerman K F 2009 Handbook of anatomical models for radiation dosimetry, Edited by Xu G and Eckerman K, *CRC Press ,Taylor & Francis,* Boca Raton, FL

Zaidi H and Xu G 2007 Computational anthropomorphic models of the human anatomy: The path to realistic Monte Carlo modeling in radiological science *Annu. Rev. Biomed. Eng.* ***9*** *471-500*

Zankl M, Veit R, Williams G, Schneider K and Fendel H 1988 The construction of computer tomographic phantoms and their application in radiology and radiation protection *Radiat. Environ. Biophys.* ***27****, 153-164*

Zankl M and Wittmann A 2001 The adult male voxel model "Golem" segmented from whole-body CT patient data *Radiat. Environ. Biophys.****40*** *153-162*

Zankl M, Fill U, Petoussi-Henss N, Regulla D 2002 Organ dose conversion coefficients for external photon irradiation of male and female voxel models *Phys. Med. Biol.* ***47****, No.14, 2367-2386*

Zankl M, Eckerman K F and Bolch W E 2007 Voxel-based models representing the male and female ICRP reference adult—the skeleton *Rad. Prot. Dos.* ***127*** *174-186*

Zhang B, Ma J, Liu L and Cheng J 2007 CNMAN: A Chinese adult male voxel phantom constructed from color photographs of a visible anatomical data set *Rad. Prot. Dos.* ***124*** *No.2 130-136*

Zhang J Y, Na Y H and Xu XG 2008a Size Adjustable Worker Models For Improved Radiation Protection Dosimetry. *Health Phys.*, Vol **95**(1), S50

Zhang J Y, Na Y H and Xu X G 2008b Development of Whole-Body Phantoms Representing An Average Adult Male and Female Using Surface-Geometry Methods. *Med. Phys*., Vol **35**(6), 2875

Zhang J, Na Y H, Caracappa P F and Xu X G 2009 RPI-AM and RPI-AF,a pair of mesh-based, size-adjustable adult male and female computational phantoms using ICRP-89 parameters and their calculations for organ doses from monoenergetic photon beams. *Phys. Med. Biol*. **54** 5885-5908

Zubal I G, Harrell C R, Smith E O, Rattner Z, Gindi G, Hoffer P B (1994a), Computerized three-dimensional segmented human anatomy *Med.Phys.* ***21*** *No.2, 299-302*